Inclusive neutron cross sections at forward angles from Nb-Nb and Au-Au collisions at 800 MeV/nucleon

R. Madey, W.-M. Zhang, B. D. Anderson, A. R. Baldwin, M. Elaasar, B. S. Flanders,*
D. Keane, W. Pairsuwan,† J. Varga, and J. W. Watson
Kent State University, Kent, Ohio 44242

G. D. Westfall
Michigan State University, East Lansing, Michigan 44823

C. Hartnack and H. Stöcker
Institut für Theoretische Physik, J. W. Goethe Universität, D-6000 Frankfurt, Federal Republic of Germany

K. Frankel
Research Medicine and Radiation Biology Division, Lawrence Berkeley Laboratory, Berkeley, California 94720
(Received 5 March 1990)

Inclusive neutron spectra were measured at 0°, 4°, 8°, 15°, 30°, and 42° from Nb-Nb and Au-Au collisions at 800 MeV/nucleon. A peak that originates from neutron evaporation from the projectile appears in the spectra at angles out to 8°. The shapes and magnitudes of the spectra are compared with those calculated from models of nucleus-nucleus collisions. The differential cross sections for Au-Au collisions are about four times those for Nb-Nb collisions. The predictions of the Vlasov-Uehling-Uhlenbeck (VUU) and QMD theories agree with the angular distributions of the differential cross sections except at small angles; the VUU prediction overestimates the angular distributions from a few degrees to about 20°, whereas the QMD prediction underestimates the angular distributions below 8°. The Firestreak-model overestimates the angular distribution for Nb-Nb collisions and underestimates it for Au-Au collisions. Also, the VUU and QMD models agree with the measured double-differential cross sections in more angular and energy regions than the Firestreak and intranuclear cascade models; however, none of the models can account for the peaks at small angles ($\theta \leq 15°$).

I. INTRODUCTION

The equation-of-state (EOS) is fundamental for the understanding of nuclear matter away from the equilibrium and for learning about phase transitions of nuclear matter.[1,2] Efforts to extract the EOS have been based on a comparison of high-multiplicity-selected data from 4π detectors with theoretical models;[3,4] however, most of the models have not been tested in much simpler measurements of inclusive cross sections. The measurement of double-differential inclusive cross sections at forward and backward angles is an important supplement to the high-multiplicity-selected data and can help to sort our theoretical descriptions. Agreement between predictions and measurements of inclusive double-differential cross sections over a wide angular region has not been achieved for relativistic collisions of heavy nuclei. If the models cannot reproduce the inclusive spectra, the veracity of their predictions for global variables can be questioned; hence, the ability to obtain agreement remains as an important challenge in relativistic heavy-ion physics.

In this paper, we report measurement of inclusive double differential cross sections for neutron emission at 0°, 4°, 8°, 15°, 30°, and 42°, from 800-MeV/nucleon Nb-Nb and Au-Au collisions. Also, we compare the reported spectra with predictions from several models: (1) Firestreak,[5,6] (2) intranuclear cascade,[7–9] (3) Vlasov-Uehling-Uhlenbeck (VUU) transport theory,[1,4,10–12] and (4) quantum-molecular dynamics (QMD).[13–15] We find that none of these approaches can provide overall agreement with the results from this experiment.

II. APPARATUS

The data were taken at the Bevalac accelerator at the Lawrence Berkeley Laboratory. Shown in Fig. 1 is the experimental arrangement, which was described in detail previously.[16] Six mean-timed[17] neutron detectors[18] were located at 0°, 4°, 8°, 15°, 30°, and 42° with respect to the beam direction. Each detector consisted on an NE-102 plastic scintillator, 10.16 cm thick and 101.6 cm high; the scintillators at the first four foward angles were 25.4 cm wide, and those at the remaining two angles were 50.8 cm wide. Neutrons were emitted from Nb-Nb or Au-Au collisions with a projectile energy of 800 MeV/nucleon at the center of a 1.37 g/cm^2 Nb (1.71 g/cm^2 Au) target oriented at 45° with respect to the beam direction. Charged particles incident on each of the six neutron detectors were vetoed with either a 6.3-mm or a 9.5-mm thick anticoincidence plastic scintillator. The time of flight (TOF) of each detected neutron was determined by measuring the time difference between the detection in

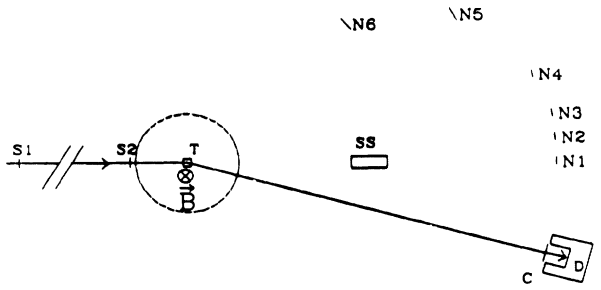

FIG. 1. Experimental arrangement. $N1$ through $N6$ represent six neutron detectors, $S1$ and $S1$ are the two scintillators of the beam telescope, T is the target, SS is one of the shadow shields, C is the centrality detector, D is the beam dump, and B shows the magnetic field of the HISS magnet.

one of the neutron detectors and the detection of a Nb (or Au) ion in a beam telescope, which consisted of two NE-102 (76.2 mm×76.2 mm×0.8 mm thick) scintillation counters positioned about 0.4 and 13 m upstream of the target. The flight paths for the six detectors decreased with increasing polar angle of the detector; they were 14.3, 14.3, 14.3, 13.9, 12.0, and 8.4 m respectively. The standard deviation in the energy resolution was estimated to be 33 MeV for an 800-MeV neutron in the detector at 0° and 5 MeV for a 200-MeV neutron in the detector at 42°. With a proton energy threshold of 20 MeV, the neutron detection efficiencies for a 50.8-cm wide detector, calculated with the Monte Carlo code of Cecil *et al.*,[19] were relatively flat at a level of 7.0% from 150 to 500 MeV and then decreased with increasing energy to about 4.2% at 2 GeV. The efficiencies for neutron energies above 500 Mev have not been tested experimentally;[18] however, as pointed out in Ref. 16, the uncertainties in the detection efficiencies do not prevent us from extracting physics results of interest. The detection efficiencies for a 25.4-cm-wide detector were calculated to be no more than 0.5% lower than those for a 50.8-cm-wide detector at all energies.

Auxiliary measurements with steel shadow shields, 152-cm long, were used to determine target-correlated backgrounds. The other dimensions were 71 cm high by 20.3 cm wide for the 25.4-cm-wide detectors, and 101 cm high by 50.8 cm wide for the 50.8-cm-wide detectors. Each shadow shield was located about half-way between the target and the detector. The shadow shields attenuated neutrons by a factor $>10^4$ at all energies. There were four configurations for shadow shields: the first configuration shadowed the detectors at 8° and 30°; the second, at 0° and 42°, the third, at 4°, and 42°, and the fourth, at 15° and 42°. To avoid contamination from backgrounds related to shadow shields, the data in a detector without a shadow shield were analyzed only if the scattering angle of neutrons from any shadow shield to that detector was larger than 16°.

The intensity of the usable incident beam was about 2×10^5 ions per pulse after a rejection loss of about 60%. Pileup circuitry rejected any beam ion that was accompanied by a second beam ion within a predetermined sampling time of typically ±400 ns. After traversing the beam telescope and the target, the beam was deflected by the large-aperture HISS magnet through an angle of 15° into a reentrant beam dump. A large (177.8 cm high ×101.6 cm wide×0.95 cm thick) scintillation counter was located in front of the beam dump. The pulse height from this centrality detector served as a tag for the degree of centrality of the collisions. As shown by Lu *et al.*,[20] large pulse heights are associated with low-multiplicity (preferentially peripheral) collisions, and small pulse heights with high-multiplicity (preferentially central) collisions. Pulse heights from the centrality detector were used to separate peripheral and central collisions and to delineate the dependence on the impact parameter[16] of the inclusive neutron spectra at 0°.

Events with two neutrons in a detector were indistinguishable from single-neutron events. Based on an auxiliary measurement,[16] the ratio R of the number of two-neutron events to the number of single-neutron events for the detector at 0° was equal to (2.5±0.5)% for Nb-Nb collisions and (11±1)% for Au-Au collisions. The values of the ratio R for other detectors, being less than a few percent, were negligible within uncertainties.

When a proton was incident on a detector at the same time as a neutron, the anticoincidence plastic scintillator vetoed that neutron. This proton-veto rate was small in this experiment because the strong magnetic field of the HISS magnet deflected most protons away from the detectors. The deflection angle θ_d of a heavy ion in a given magnetic field is proportional to Z/Ap, where Z is the charge, A is the mass number, and p is the momentum per nucleon of the ion. For an 800 MeV/nucleon Au projectile with $Z/A=79/197\approx1/2.5$, the deflection angle θ_d was designed to be 15° in this experiment; accordingly, for protons emitted at 0°, the deflection angle was about 37°. The ratio of the neutron differential cross section at 37° to that at 0° was observed to be less than 1% for Au-Au collisions; thus, the proton-veto rate for the detector at 0° is estimated to be less than 4% after multiplying this cross-section ratio of less than 1% by the estimated[16] neutron-hit rate of six per event for the detector at 0° and dividing by the neutron-to-proton ratio of 1.5. In a similar way, the proton-veto rates at other angles are estimated to be less than the 4% rate at 0°. Because other charged particles are emitted less copiously than protons, the veto rates from other charged particles are small compared to the proton-veto rate. For Nb-Nb collisions, the veto rates from protons or other charged particles were even smaller than those for Au-Au collisions because of the smaller cross sections for Nb-Nb collisions.

III. INCLUSIVE SPECTRA

The kinetic energy of each neutron was derived from the measured TOF. Inclusive double-differential cross sections are plotted as a function of the neutron laboratory kinetic energy in Figs. 2 and 4 for Nb-Nb collisions and in Figs. 3 and 5 for Au-Au collisions. The cross sections at 0°, 8°, and 30° are shown in Figs. 2 and 3; and those at 4°, 15°, and 42° in Figs. 4 and 5. Because of large

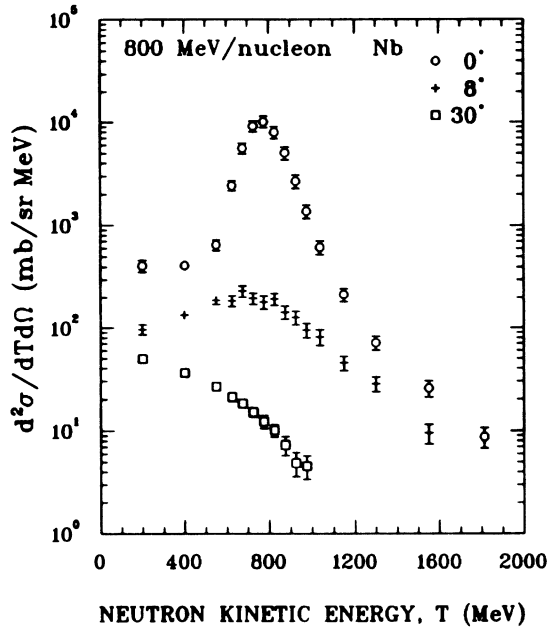

FIG. 2. The inclusive double-differential cross sections for neutron emission at 0°, 8°, and 30° from Nb-Nb collisions at 800 MeV/nucleon vs the neutron kinetic energy in the laboratory.

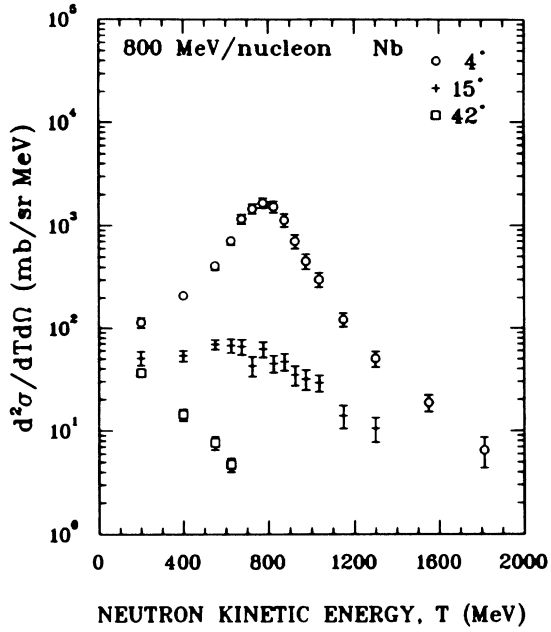

FIG. 4. The inclusive double-differential cross sections for neutron emission at 4°, 15°, and 42° from Nb-Nb collisions at 800 MeV/nucleon vs the neutron kinetic energy in the laboratory.

uncertainties from background subtractions, the data points below 4.0 mb/MeV sr in Figs. 2 and 4 are excluded. In Figs. 2 through 5 for the six forward angles, the energy bin width at low and high energies is chosen to be larger than that in the region of the peak in order to maintain comparable statistical uncertainties over the whole range from 200 MeV to 2 GeV. The spectra at 0°, which were discussed in detail in Ref. 16 are characterized by a high-energy tail and a peak at an energy of 753±30 MeV for Nb-Nb collisions and 731±30 MeV for Au-Au collisions. The spectra at 4° from both Nb-Nb

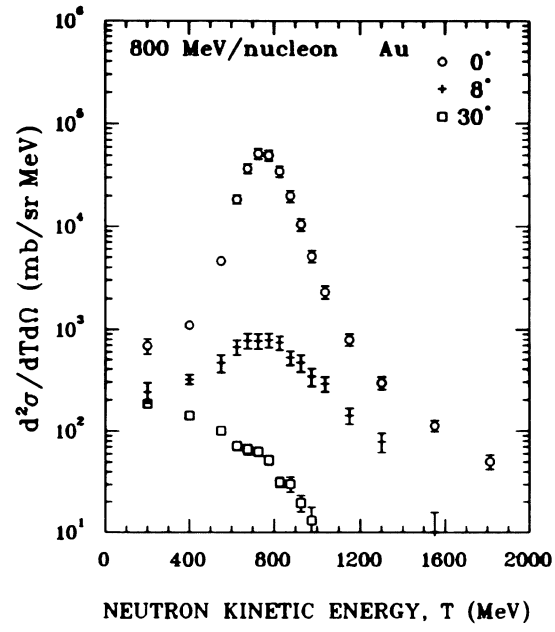

FIG. 3. The inclusive double-differential cross sections for neutron emission at 0°, 8°, and 30° from Au-Au collisions at 800 MeV/nucleon vs the neutron kinetic energy in the laboratory.

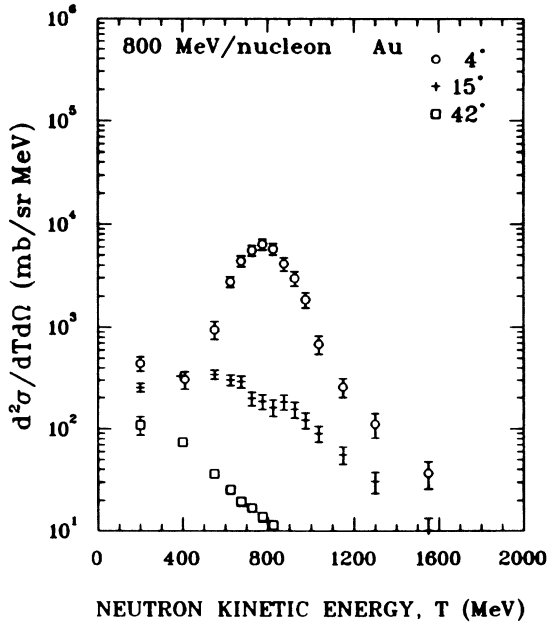

FIG. 5. The inclusive double-differential cross sections for neutron emission at 4°, 15°, and 42° from Au-Au collisions at 800 MeV/nucleon vs the neutron kinetic energy in the laboratory.

and Au-Au collisions are similar to those at 0° in that they show a high-energy tail and a peak which is located at about the same position as that at 0°. The high-energy tail in the spectra at 4° is believed[16] to result from backscattering of neutrons in the target from clusters in the projectile, which is the same interpretation given to the spectra at 0°;[16] at 4°, however, the backscatterings deviate slightly from the beam direction. As indicated in Ref. 16 for the peak at 0°, the peak in the spectra at 4° arises also from neutron evaporation from the projectile. These evaporation neutrons arise from peripheral collisions. A small and broad peak in the spectra at 8° from both Nb-Nb and Au-Au collisions implies the evaporation neutrons can be emitted from the projectile at an angle as wide as 8° in the laboratory.

The neutron double-differential cross sections at 0° through 42° were integrated over neutron kinetic energies above 200 Mev. Plotted together in Fig. 6 are the angular distributions of the differential cross sections for emission of neutrons above 200 MeV from Nb-Nb (circle) and Au-Au (squares) collisions. The total neutron cross sections $\sigma(T>200$ MeV, $0°\le\theta\le42°)$ were obtained by integrating the above differential cross sections over the polar angle region from 0° to 42°; the results are 76 ± 10 b for Nb-Nb collisions and 315 ± 38 b for Au-Au collisions. Exclusion of the polar angle region from 42° to 180° neglects $(20\pm4)\%$ of the total cross sections for both Nb-Nb and Au-Au collisions. The missing cross sections were estimated from exponential extrapolations of the three points (at 15°, 30°, and 42°) of the angular distributions in Figs. 6. The ratio $\sigma(T>200$ MeV, $0°\le\theta\le42°)/4\pi R^2$, where R is the radius of the nucleus, is 21 ± 3 and 52 ± 7 for Nb-Nb and Au-Au collisions, respectively, indicating that the average neutron multiplicity in this chosen fiducial region is about one-fifth of the number of neutrons in the projectile plus the target.

Comparison of the two angular distributions in Fig. 6 shows that the neutron double-differential cross sections for Au are about four times those for Nb. This factor of 4 is equal approximately to the ratio (≈3.7) of the product of the neutron number and the geometric reaction cross section. This interpretation indicates that the neutron double-differential cross section from collisions of two heavy nuclei with equal masses is proportional to the number of neutrons in the nucleus.

The error bars shown in the figures include both the statistical and the estimated systematic uncertainties. As described in Ref. 16 for the spectra at 0°, the systematic uncertainty from the determination of the proton energy threshold is about 10% in the spectra at the six forward angles. The statistical uncertainty in the spectra at the six forward angles is smaller than this 10% systematic uncertainty at energies below about 800 MeV; it increases with increasing neutron energy to about 20% for Au-Au collisions and about 40% for Nb-Nb collisions at the highest neutron energies shown in the spectra.

The measurements of inclusive neutron spectra at the six forward angles are plotted in Figs. 7 and 8 as contours of Lorentz-invariant cross sections for Nb-Nb and Au-Au collisions, respectively, in the space of transverse momen-

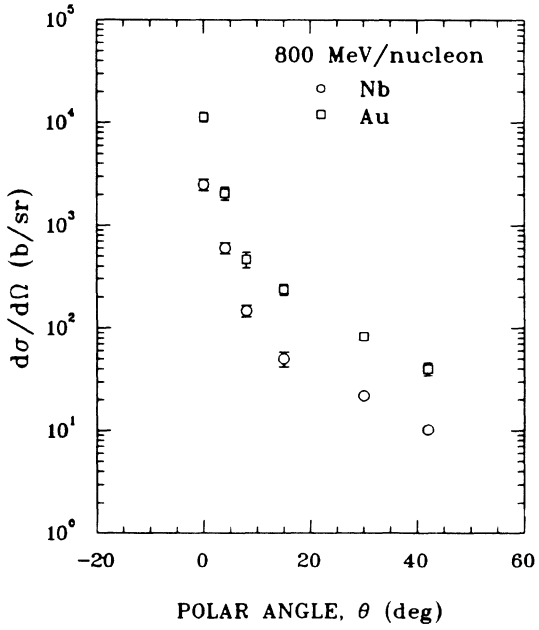

FIG. 6. The inclusive differential cross section for emission of neutrons above 200 MeV from Nb-Nb (circles) and from Au-Au (squares) collisions at 800 MeV/nucleon vs the emission angle.

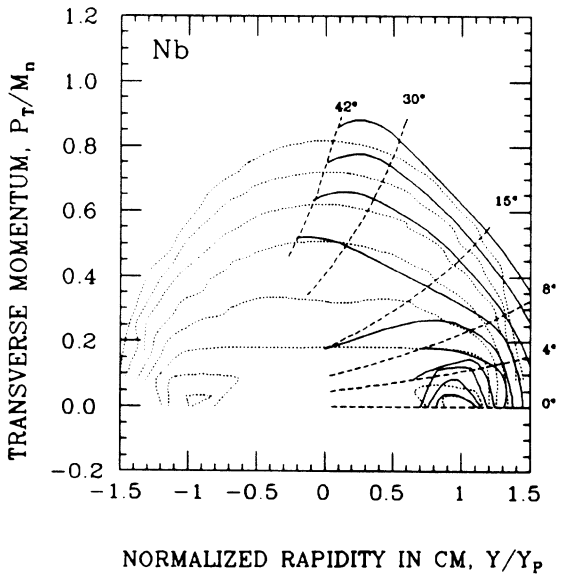

FIG. 7. Contours of Lorentz-invariant cross sections for emission of neutrons from Nb-Nb collisions at 800 MeV/nucleon plotted in the plane of transverse momentum (normalized to the mass of neutron) vs the neutron rapidity in center-of-mass system (normalized to the projectile rapidity). The solid lines represent the data. The dotted lines are QMD calculations. The successive contours increase by a multiplicative factor of 2; the values of the Lorentz-invariant cross sections are 5 $\mu b\, c^3/\mathrm{MeV}^2$ sr for the outermost contour and 2,560 $\mu b\, c^3 \mathrm{MeV}^2$ sr for the innermost contour.

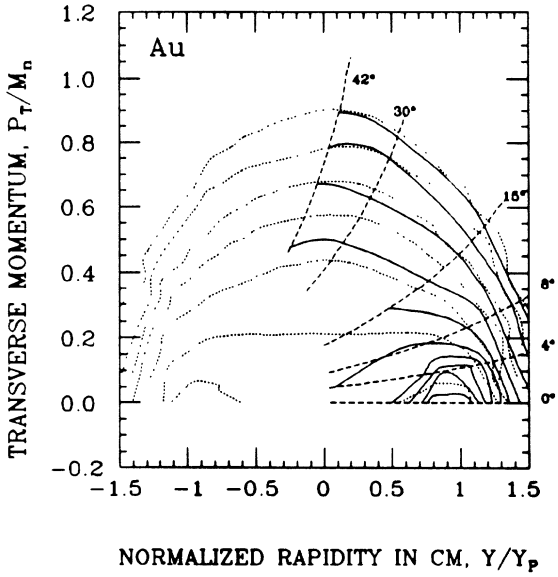

FIG. 8. Contours of Lorentz-invariant cross sections for emission of neutrons from Au-Au collisions at 800 MeV/nucleon plotted in the plane of transverse momentum (normalized to the mass of neutron) vs the neutron rapidity in the center-of-mass system (normalized to the projectile rapidity). The solid lines represent the data. The dotted lines are QMD calculations. The successive contours increase by a multiplicative factor of 2; the values of the Lorentz-invariant cross sections are 20 $\mu b\, c^3/\mathrm{MeV}^2\,\mathrm{sr}$ for the outermost contour and 10 240 $\mu b\, c^3/\mathrm{MeV}^2\mathrm{sr}$ for the innermost contour.

tum P_T (normalized to the neutron mass M_n) versus the neutron rapidity Y (normalized to the projectile rapidity Y_P) in the center-of-mass system. The cross section values on successive contours in each of these figures increase by a multiplicative factor of 2. In Fig. 7 for Nb, the values of the Lorentz-invariant cross sections are 5 $\mu b\, c^3/\mathrm{MeV}^2\,\mathrm{sr}$ for the outermost contour and 2 560 $\mu b\, c^3/\mathrm{MeV}^2\,\mathrm{sr}$) for the innermost contour. The corresponding values are four times larger in Fig. 8 for Au. The dashed lines in the two figures represent the phase-space of neutrons detected in the six detectors from 0° to 42°, respectively. The extremities of these lines denote the upper and lower limits of the momenta detected in the experiment. From the two figures, we see contours centered around a value of the normalized rapidity that is slightly smaller than the projectile rapidity of $Y/Y_p = 1$; these contours are produced by spectator neutrons emitted from the projectile. Also, we see contours centered at zero rapidity formed by participant neutrons. Plotted in Figs. 7 and 8 with dotted lines are predictions of contours in the full phase space from the QMD model.[13–15] We find that the data and the predictions from the QMD model agree within a factor of 2 in the reion of positive rapidities up to about 1.2 and normalized transverse momenta P_T/M_N above about 0.15. The higher observed cross sections at $P_T/M_n < 0.15$ in the vicinity of the projectile rapidity can be explained by the fact that the QMD model does not include neutron evaporation which dominates the cross sections in this region.[16] Because none of the models discussed in the next section include neutron evaporation, predictions from these models do not account for the evaporation component seen in the spectra at the most forward angles.

IV. COMPARISON WITH MODELS

Here we compare the results from this experiment with four models of nucleus-nucleus collisions: Firestreak, intranuclear cascade, VUU, and QMD. The Firestreak model is a modified version of the Fireball model.[21] At angles where thermal processes dominate, Firestreak cross sections agree reasonably well with spectra at bombarding energies in the vicinity of a few hundred MeV per nucleon, and with spectra from collisions of light-mass systems only at higher bombarding energies up to about 1 GeV per nucleon.[5] The dynamical input is minimal in Firestreak. The VUU model[1,10] is a microscopic transport theory that is a Monte Carlo solution of the Vlasov-Uehling-Uhlenbeck (VUU) equation.[10] It proceeds in terms of a cascade of binary collisions between nucleons, resonances, and pions according to the experimental scattering cross sections for free particles, corrected by a Pauli blocking factor. The isospin of each particle is incorporated explicitly. The dependence on the EOS enters via the acceleration of nucleons in the nuclear mean field. The VUU model predicts both collective flow and nucleon cross sections from collision of various systems at different beam energies;[4,11–12] however, because the VUU approach does not account for the formation of composite nuclei, we expect the VUU theory to overestimate the measured nucleon cross sections. The intranuclear cascade model does not include compressional energy, and it calculates the number of free neutrons by subtracting the number of deuteron-like pairs[22] from all neutrons including those in clusters. The QMD theory combines the quantum features of the VUU theory with a long-range N-body interaction, and it takes composites into account.[13–15] It is of interest to compare the predictions of these models with the measured differential cross sections. The spectra measured in this experiment will test these models for collisions of heavy-mass systems such as Nb-Nb and Au-Au at an energy of 800 MeV/nucleon. A similar comparison was done for collisions of La-La at an energy of 800 MeV/nucleon.[23]

Predictions of the angular distributions from 0° to 60° of the differential cross sections are shown in Fig. 9 for Nb-Nb collisions and in Fig. 10 for Au-Au collisions. Predictions, from the Firestreak, VUU, and QMD models are represented, respectively, by solid, dashed, and dotted lines in Figs. 9 and 10. The statistical uncertainties in the Monte Carlo calculations are smaller than the total uncertainties in the measurements. Because the intranuclear cascade code calculates too many deuterons at low energies as a result of contributions from higher-mass composites, it does not yield reliable predictions of double-differential cross sections at low energies; therefore, the intranuclear cascade model calculations of these angular distributions are not presented here. The VUU

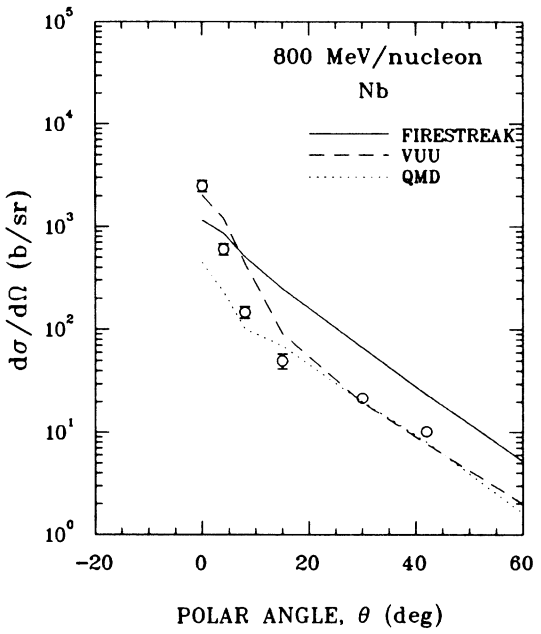

FIG. 9. Predictions for the inclusive differential cross section for the emission of neutrons above 200 MeV from Nb-Nb collisions at 800 MeV/nucleon vs the laboratory emission angle. Solid, dashed, and dotted lines represent predictions from Firestreak, VUU, and QMD models, respectively. Symbols denote the data.

code used here was developed by H. Stöcker *et al.*[11] Because VUU calculations made here with both supersoft and stiff EOS yielded the same results, the spectra presented here present the sum of both calculations. From Figs. 9 and 10, we see that the predictions of the VUU and QMD theories agree with the magnitude of the differential cross sections at larger angles; at small angles, the VUU prediction overestimates the angular distributions from a few degrees to about 20°, and the QMD prediction underestimates the angular distributions below 8°. Also, we see that the Firestreak model overestimates the angular distribution for Nb-Nb collisions and underestimates it for Au-Au collisions.

For double-differential cross sections at six polar angles, we find that VUU and QMD models agree with the data in more angular and energy regions than the Firestreak and intranuclear cascade models, but that none of these models can account for the peaks at small angles ($\theta \leq 15°$); as examples, we present here the comparison of our measurements at three representative angles (viz., 4°, 15°, and 42°) with the predictions from the four models. Predictions for the double-differential cross sections at 4°, 15°, and 42° are plotted in Figs. 11, 12, and 13, respectively, for Nb-Nb collisions and in Figs. 14, 15, and 16 for Au-Au collisions. In Figs. 11–16, solid, dashed, dotted, and dot-dashed lines represent predictions from Firestreak, VUU, QMD, and intranuclear cascade models, respectively. The comparisons of the calculated spectra with measured neutron spectra at 4° in Fig. 11 for Nb and

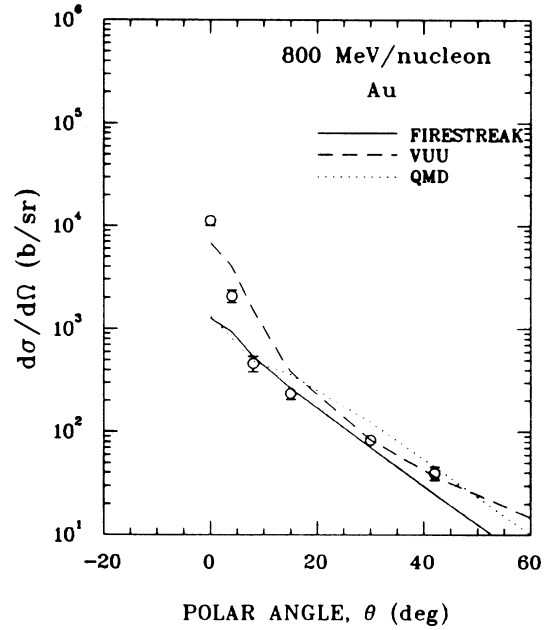

FIG. 10. Predictions for the inclusive differential cross section for the emission of neutrons above 200 MeV from Au-Au collisions at 800 MeV/nucleon vs the laboratory emission angle. Solid, dashed, and dotted lines represent predictions from Firestreak, VUU, and QMD models, respectively. Symbols denote the data.

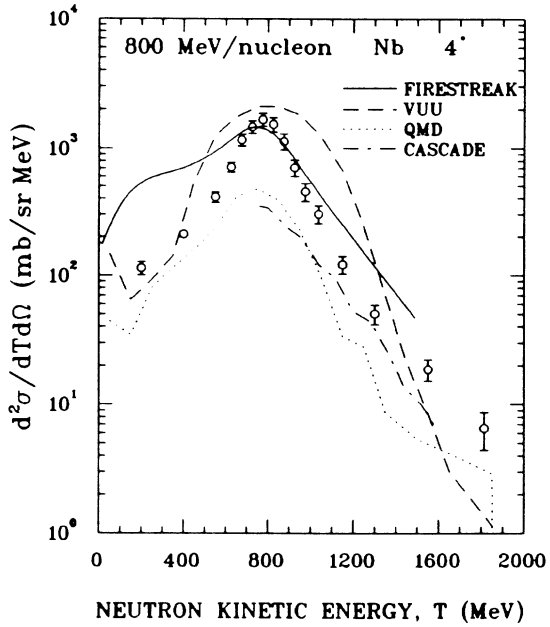

FIG. 11. Predictions for the inclusive double-differential cross sections for neutron emission at 4° from Nb-Nb collisions at 800 MeV/nucleon vs the neutron kinetic energy in the laboratory. Solid, dashed, dotted, and dot-dashed lines represent predictions from Firestreak, VUU, QMD, and cascade models, respectively. Symbols denote the data.

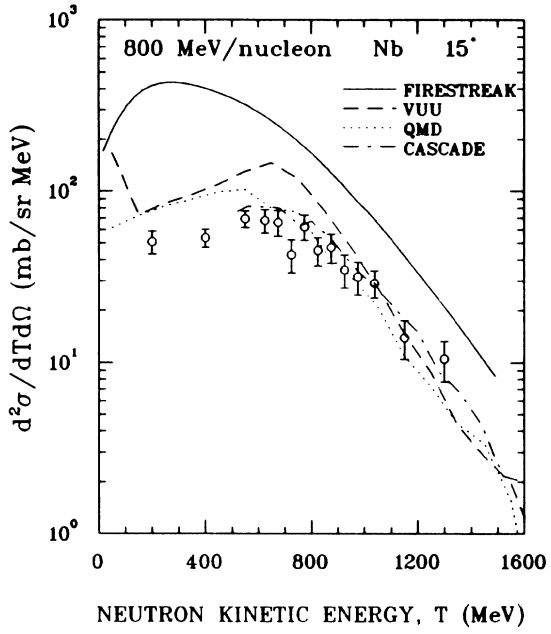

FIG. 12. Predictions for the inclusive double-differential cross sections for neutron emission at 15° from Nb-Nb collisions at 800 MeV/nucleon vs the neutron kinetic energy in the laboratory. Solid, dashed, dotted, and dot-dashed lines represent predictions from Firestreak, VUU, QMD, and cascade models, respectively. Symbols denote the data.

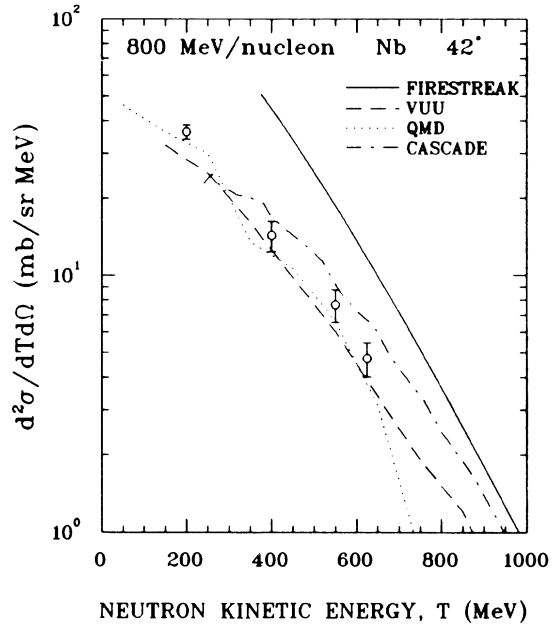

FIG. 13. Predictions for the inclusive double-differential cross sections for neutron emission at 42° from Nb-Nb collisions at 800 MeV/nucleon vs the neutron kinetic energy in the laboratory. Solid, dashed, dotted, and dot-dashed lines represent predictions from Firestreak, VUU, QMD, and cascade models, respectively. Symbols denote the data.

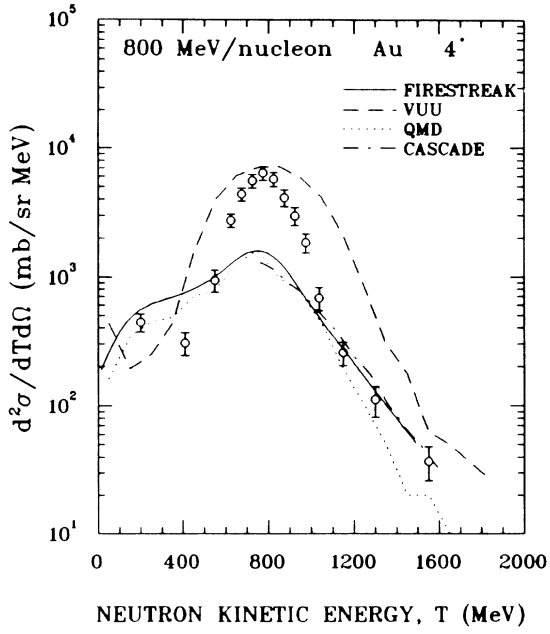

FIG. 14. Predictions for the inclusive double-differential cross sections for neutron emission at 4° from Au-Au collisions at 800 MeV/nucleon vs the neutron kinetic energy in the laboratory. Solid, dashed, dotted, and dot-dashed lines represent predictions from Firestreak, VUU, QMD, and Cascade models, respectively. Symbols denote the data.

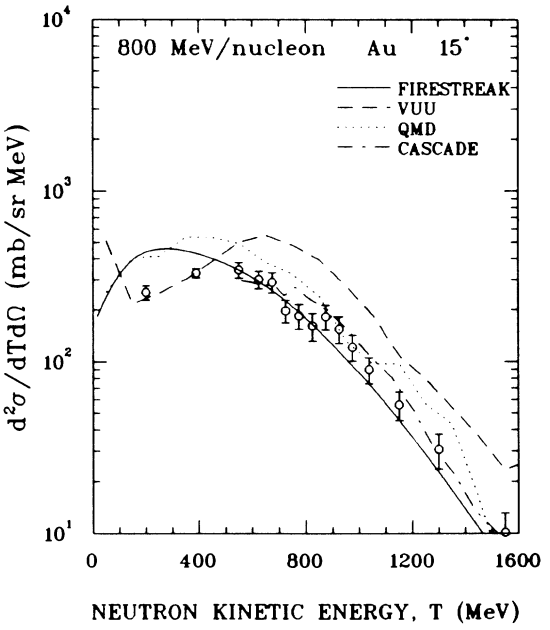

FIG. 15. Predictions for the inclusive double-differential cross sections for neutron emission at 15° from Au-Au collisions at 800 MeV/nucleon vs the neutron kinetic energy in the laboratory. Solid, dashed, dotted, and dot-dashed lines represent predictions from Firestreak, VUU, QMD, and cascade models, respectively. Symbols denote the data.

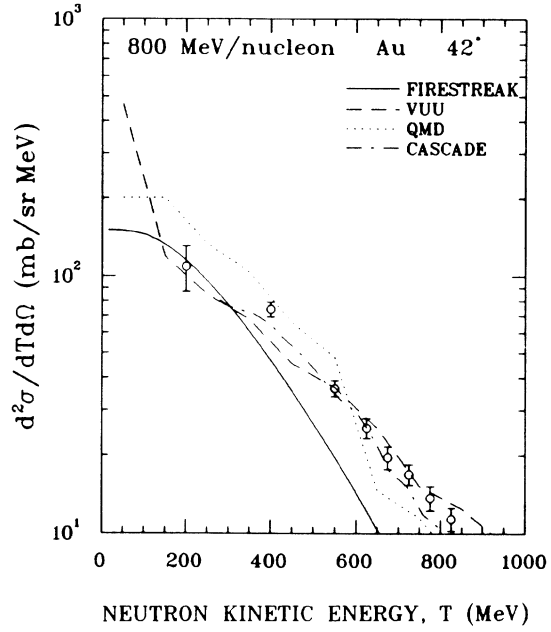

FIG. 16. Predictions for the inclusive double-differential cross sections for neutron emission at 42° from Au-Au collisions at 800 MeV/nucleon vs the neutron kinetic energy in the laboratory. Solid, dashed, dotted, and dot-dashed lines represent predictions from Firestreak, VUU, QMD, and cascade models, respectively. Symbols denote the data.

in Fig. 14 for Au show that a good description of cluster formation and neutron evaporation is needed to account for the measured spectra. The fact that the data lie between the predictions of the VUU and QMD models demonstrates the importance of cluster formation in the high cross section region (i.e., the region of high phase space density). Because the VUU calculation includes too many free neutrons by not subtracting those that coalesce into clusters, the VUU calculation predicts higher cross sections than those observed; conversely, because the QMD calculation includes too few free neutrons by not accounting for the evaporation of neutrons from excited clusters, the QMD calculation predicts lower cross sections than those observed. The large number of evaporation neutrons seen in the data in the region of the peaks at 0° and 4° indicates that many excited clusters are created in peripheral collisions. A measurement of these clusters would be of interest.

V. CONCLUSIONS

We measured inclusive neutron spectra at six forward angles 0°, 4°, 8°, 15°, 30°, and 42° from Nb-Nb and Au-Au collisions at 800 MeV/nucleon. Neutrons evaporated from an excited projectile appear in the spectra at angles up to 8°. Comparisons of the spectra with predictions from the Firestreak, VUU, QMD, and intranuclear cascade models show that none of these models agree with the spectra of the double-differential cross sections at all angles for both Nb-Nb and Au-Au collisions. Also, predictions of the angular distributions of the differential cross sections do not agree with the measurements over the full angular range; the better representations come from the VUU and QMD models. In the region of the projectile rapidity where the cross section is the highest, the difference between the VUU and QMD calculations demonstrates the importance of cluster formation. It is necessary to account for the removal of neutrons bound in clusters and for the evaporation of neutrons from the excited clusters.

ACKNOWLEDGMENTS

We are grateful for the support of the Ohio Supercomputer Center for providing facilities that make theoretical simulations possible. This work was supported in part by the National Science Foundation under Grant Nos. PHY-88-02392, PHY-85-01054, and PHY-86-11210, and by the U.S. Department of Energy under Contract Nos. DE-FG89ER40531 and DE-AC03-76SF00098.

*Present address: American University, Washington, D.C. 20016.

†Present address: Fast Neutron Facility, Chiang Mai University, Chiang Mai, 50002, Thailand.

[1]H. Stöcker and W. Greiner, Phys. Report **137**, 278 (1986).

[2]R. Stock, Nature **337**, 319 (1989).

[3]K. G. R. Doss, H. Å. Gustafsson, H. H. Gutbrod, K. H. Kampert, B. Kolb, H. Löhner, B. Ludewigt, A. M. Poskanzer, H. G. Ritter, H. R. Schmidt, and H. Wieman, Phys. Rev. Lett. **57**, 302 (1986).

[4]D. Keane, S. Y. Chu, S. Y. Fung, Y. M. Liu, L. J. Qiao, G. VanDalen, M. Vient, S. Wang, J. J. Molitoris, and H. Stöcker, Phys. Rev. C **37**, 1447 (1988); P. Danielewicz, H. Ströbele, G. Odyniec, D. Bangert, R. Bock, R. Brockmann, J. W. Harris, H. G. Pugh, W. Rauch, R. E. Renfordt, A. Sandoval, D. Schall, L. S. Schroeder, and R. Stock, *ibid.* **38**, 120 (1988).

[5]W. D. Myers, Nucl. Phys. **A296**, 177 (1978).

[6]J. Gosset, J. I. Kapusta, and G. D. Westfall, Phys. Rev. C **18**, 844 (1978).

[7]Y. Yariv and Z. Fraenkel, Phys. Rev. C **24**, 488 (1981).

[8]J. Cugnon, D. Kinet, and J. Vandermeulen, Nucl. Phys. **A379**, 553 (1982).

[9]J. Cugnon and D. L'Hôte, Phys. Lett. **149B**, 35 (1984).

[10]E. A. Uehling and G. E. Uhlenbeck, Phys. Rev. **43**, 552 (1933).

[11]H. Kruse, B. V. Jacak, and H. Stöcker, Phys. Rev. Lett. **54**, 289 (1985); and H. Kruse, B. V. Jacak, J. J. Molitoris, G. D. Westfall, and H. Stöcker, Phys. Rev. C **31**, 1770 (1985).

[12]J. J. Molitoris and H. Stöcker, Phys. Rev. **C32**, 346 (1985).

[13]J. Aichelin and H. Stöcker, Phys. Lett. B **176**, 14 (1986).

[14]A. Rosenhauer *et al.*, Phys. (Paris) C **4**, 395 (1986).

[15]J. Aichelin, A. Rosenhauer, G. Peilert, H. Stöcker, and W. Greiner, Phys. Rev. Lett. **58**, 1926 (1987).

[16]R. Madey, W.-M. Zhang, B. D. Anderson, A. R. Baldwin, B. S. Flanders, W. Pairsuwan, J. Varga, J. W. Watson, and G. D.

Westfall, Phys. Rev. C **38**, 184 (1988).
[17]A. R. Baldwin and R. Madey, Nucl. Instrum. Methods **171**, 149 (1980).
[18]R. Madey, J. W. Watson, M. Ahmad, B. D. Anderson, A. R. Baldwin, A. L. Casson, W. Casson, R. A. Cecil, A. Fazely, J. M. Knudson, C. Lebo, W. Pairsuwan, P. J. Pella, J. C. Varga, and T. R. Witten, Nucl. Instrum. Methods **214**, 401 (1983).
[19]R. A. Cecil, B. D. Anderson, and R. Madey, Nucl. Instrum. Methods **161**, 439 (1979).
[20]J. J. Lu, D. Beavis, S. Y. Fung, W. Gorn, A. Huie, G. P. Kiernan, R. T. Poe, and G. VanDalen, Phys. Rev. Lett. **46**, 898 (1981).
[21]G. D. Westfall, J. Gosset, P. J. Johansen, A. M. Poskanzer, W. G. Meyer, H. H. Gutbrod, A. Sandoval, and R. Stock, Phys. Rev. Lett. **37**, 1202 (1976).
[22]G. Bertsch and J. Cugnon, Phys. Rev. C **24**, 2514 (1981).
[23]J. Aichelin, J. Cugnon, Z. Fraenkel, K. Frankel, C. Gale, M. Gyulassy, D. Keane, C. M. Ko, J. Randrup, A. Rosenhauer, H. Stöcker, G. Welke, and J. Q. Wu, Phys. Rev. Lett. **62**, 1461 (1989).